Real-Time Multirate State Estimation in a Pilot-Scale Polymerization Reactor

Neeraj Zambare and Masoud Soroush
Dept. of Chemical Engineering, Drexel University, Philadelphia, PA 19104

Michael C. Grady
Marshall Laboratory, E.I. duPont de Nemours Co., Philadelphia, PA 19146

Real-time implementation of a robust multirate state estimator on a continuous stirred-tank, free-radical, styrene polymerization reactor is presented. The estimator is designed based on a first-principles model of the process. It has integral action that allows for robust estimation of the process states. The estimator calculates frequent robust estimates of polymer weight-average and number-average molecular weights and monomer concentration. These are estimated from frequent online measurements of the reactor temperature, and infrequent offline and delayed measurements of polymer weight-average and number-average molecular weights and monomer concentration. Infrequent measurements of monomer concentration are obtained by gas chromatography and gravimetry, and those of weight-average and number-average molecular weights by gel permeation chromatography.

Introduction

Effective control and monitoring of a process require sufficient frequent information on the essential variables of the process. In many cases, however, the required frequent information is not available (Bastin and Dochain, 1990; Ogunnaike, 1994a). For example, average molecular weights in polymerization reactors, biomass concentration in biochemical reactors, and overhead and bottoms composition in certain distillation columns are not measured or are measured infrequently. Furthermore, some measurements are made by using analysis methods that inherently take a considerable amount of time, and therefore are available after long time delays. Examples are molecular-weight distribution measurements obtained by gel permeation chromatography. As in control where larger measurement time delays and sampling periods have more degrading effects on the quality of control, in estimation, the quality of estimation decreases, as the measurement time delay or sampling period increases.

In many processes, measurements are available at multiple rates; some measurements are available frequently and the others infrequently (Bastin and Dochain, 1990; Stone et al. 1992; Tatiraju et al., 1999a,b). Processes with frequent (fast) and infrequent (slow) measurements have been referred to as "multirate" processes. The challenge in estimation in such processes is to design estimators that are robust against model uncertainties and unknown disturbances and that can use both fast and slow measurements effectively.

Multirate extended Kalman filters (EKFs) have been used widely for many processes. For example, Elicabe et al. (1995) applied the standard linear Kalman filter algorithm to a simple model developed for a class of semicontinuous reactors. The developed estimation algorithm was applied to the experimental data collected during the semibatch polymerization of two ternary systems to estimate the mass of each reactant and also reaction rates (to improve robustness). Ellis et al. (1988) implemented an extended Kalman filter on a 1.5-L, methyl methacrylate, batch polymerization reactor. Frequent measurements of temperature, monomer, and initiator conversion, and infrequent, delayed measurements of molecular-weight distribution (MWD) were used for the estimation. Conversion measurements were inferred from online, frequent density measurements. The same authors also used the estimator for controlling MWD in batch polymerization (Ellis et al., 1994). Radhakrishnan and coworkers (1994) used a Kalman predictor-based multirate estimator for simulated control of two distillation columns. Ogunnaike (1994b) used a modified EKF for online multirate estimation of process variables in a terpolymerization reactor. The estimator was used for online predictive control of the reactor. A significant re-

Correspondence concerning this article should be addressed to M. Soroush.

duction in product variability, for such a complex reactor, was achieved by using this estimator. Mutha and coworkers proposed a multirate measurement-based estimator using a fixed-lag smoothing-based EKF algorithm. The proposed algorithm was demonstrated to be superior to the basic EKF by using a simulation study on a complex emulsion copolymerization batch process (Mutha et al., 1997a). The algorithm was later used in an experimental estimation and control study on a methyl methacrylate solution polymerization reactor (Mutha et al., 1997b). Their algorithm could handle several measurements with different amounts of delay and variable measurement delay. Since biotechnology abounds in processes with multirate measurements, multirate state and parameter estimation in these processes has received considerable attention. For example, Gudi (1994) presented a multirate state and parameter estimator with EKF backbone, and used it for estimation in a simulated antibiotic fermentation reactor. They included as many past frequent measurements of carbon dioxide evolution rate as the number of system delays in the measurement vector to improve the observability properties of the system. This modification did improve the performance of the estimator in the face of measurement delays. However, the estimation method cannot account for variable-measurement time delay. They later experimentally applied the estimator on a fed-batch fermentation system (Gudi et al., 1995). The estimator was also used for estimation and control of nutrient levels in a fed-batch fermentation, along with some case-specific modifications (Gudi et al., 1997).

Exponential observers have also been used for multirate state estimation. Lombardi et al. (1999) presented an online application of a hybrid nonlinear observer to a continuous-stirred membrane bioreactor. A nonlinear observer proposed by the authors was used for a part of the system, whereas the exponential observer of Gauthier et al. (1992) was used for the remaining subsystem. The observer used infrequent measurements of lactic acid, biomass, and lactose concentrations to estimate the states of the process. The estimates agreed well with the experimental data. The observer, however, diverged at the end of the process due to a less accurate process model, as reasoned by the authors. Farza et al. (1999) used a modified form of the exponential observer so that the tuning of the estimator does not involve solving complex Riccati equations. The work also demonstrated experimental application to estimate states and reaction rates of lactic acid production in batch process, and esterification reaction rate and states of a reaction calorimeter. A drawback of this method is that specific parameters for a given process need to be identified for robust estimation. The observer developed by Bastin and Dochain (1986, 1990) has also been used for multirate estimation in biochemical reactors. Acuna et al. (1994) applied the nonlinear reduced-order estimator experimentally for online estimation of biological variables during pH-controlled lactic acid fermentations. Indirect offline measurements of biomass concentration were introduced into the estimator to estimate the state variables. Parameters, like specific growth and lactic acid production rates, were simultaneously estimated to improve the estimator robustness. Good agreement was found between estimated and measured biomass concentrations. Dochain et al. (1988) used the estimation algorithm online to estimate biomass concentration in a biochemical reactor. Indirect measurements of biomass concentration were used in the algorithm. Again, specific growth rate was estimated to improve robustness of the estimator. The estimator algorithm had a built-in noise-measurement filter. The estimated values of biomass concentration agreed well with the experimental values. Claes and Van Impe (1999) implemented the estimation algorithm on a biochemical reactor to simultaneously estimate the biomass concentration and specific growth rate by using online viable biomass measurements. Von Schalien et al. (1995) estimated the states of an aerobic *Saccharomyces cerevisiae* fermentation process by using a simple model-based estimator along with indirect measurements of the states. Online estimation of parameters in the transport and kinetic expressions using recursive regression analysis was used to improve robustness of the estimator. The model predictions agreed well with direct state measurements obtained by a high-performance liquid chromatograph (HPLC). However, a slight divergence was observed at the end of the fermentation.

Other approaches to multirate state estimation include multirate, nonlinear, reduced-order state observer design (Tatiraju et al., 1999a,b), and moving-horizon state estimation (Robertson et al., 1996; Russo and Young, 1999). Tatiraju and coworkers (Tatiraju et al., 1999a,b) developed a method of multirate nonlinear state observer design and applied the method to a polymerization reactor and a pilot-scale biochemical reactor in which cultivation of mouse–mouse hybridoma cells takes place. Specific growth rate and concentrations of viable cells, total cells, glucose, glutamine, and monoclonal antibodies (MAb) were estimated in the bioreactor. Urretabizkaia et al. (1994) presented a closed-loop strategy for terpolymer composition control in semicontinuous emulsion polymerization. In this strategy, a nonlinear optimization algorithm with long horizon was used to correct the state estimates as online state measurements became available. Russo and Young (1999) presented a study involving application of moving-horizon state estimation to an industrial polymerization process. A simple objective function was minimized to achieve convergence. Monomer composition, comonomer composition, temperature, and hydrocarbon effluent measurements were estimated by using their infrequent measurements. More references on state estimation can be found in review papers (Elicabe et al., 1995; Embirucu et al., 1996; James et al., 2000).

This article presents a real-time implementation of the robust multirate reduced-order nonlinear estimator proposed by Zambare et al. (2002) on a polymerization reactor in DuPont's Marshall Laboratory. The estimator calculates robust, frequent estimates of polymer weight-average and number-average molecular weights, and monomer concentration. These are estimated from (i) online frequent measurements of the reactor temperature, and (ii) offline infrequent and delayed measurements of weight-average and number-average molecular weights and monomer concentration. The infrequent measurements of monomer concentration are obtained by gas chromatography and gravimetry, and those of weight-average and number-average molecular weights by gel permeation chromatography. Unlike other estimators just mentioned, the robustness of the estimator of Zambare et al. (2002) to model uncertainties and unknown disturbances is not case-specific.

The article is organized as follows. The next section provides a brief review of the multirate estimation method. The third section describes the process and the experimental system used for the study. The fourth section presents a first-principles mathematical model for the reactor. Parameter estimation and model validation results are presented in the fifth section. The design of the robust estimator for the reactor is given in the sixth section. Finally, the seventh section presents the real-time estimation results.

Robust Multirate State Estimator Design Method

This section describes briefly the continuous-time analog of the discrete-time, robust, multirate, nonlinear state estimation method presented in (Zambare et al., 2002). Consider the class of nonlinear continuous-time processes in the form

$$\begin{aligned} \dot{x}(t) &= f[x(t), u(t)] \\ y_i(t) &= h_i[x(t)] \qquad i = 1, \ldots, p \\ Y_i(t_{ib}) &= H_i[x(t_{ib} - \theta_i)], \quad i = 1, \ldots, q;\ b = 1, 2, \ldots, \end{aligned} \tag{1}$$

where $x = [x_1, \cdots, x_n]^T$ denotes the vector of state variables; $u = [u_1, \cdots, u_m]^T$ represents the vector of measurable (manipulated) inputs; $y = [y_1, \cdots, y_p]^T$ is the vector of "fast" measurable outputs (whose measurements are available so frequently that they can be considered as continuous functions of time); $Y = [Y_1, \cdots, Y_q]^T$ is the vector of "slow" measurable outputs (whose measurements are available at lower sampling rates and with different time delays); $t_{ib} (b = 1, 2, , \cdots,)$ are the time instants at which the measurements of the slow measurable output Y_i are available; θ_i is the dead-time associated with the slow measurable output Y_i; and $f(. , .)$, $h(.) = [h_1(.), \cdots, h_p(.)]^T$, and $H(.) = [H_1(.), \cdots, H_q(.)]^T$ are smooth vector functions. Note that the infrequent measurements can be sampled irregularly (sampling period of each slow measurement can change with time).

We make the following assumptions:

(A1) The $p \times n$ matrix $\partial h(x)/\partial x$ has p locally linearly independent rows or columns; this condition ensures that none of the available fast measurable outputs are redundant.

(A2) The process state variables are at least locally detectable from the fast and slow measurable outputs.

(A3) The process state variables are at least locally *integral detectable* (Zambare et al., 2002) from the measurable outputs.

Because of assumption A1, one can always find a locally invertible state transformation of the form

$$\begin{bmatrix} \eta \\ y \end{bmatrix} = \mathfrak{I}(x) = \begin{bmatrix} Qx \\ h(x) \end{bmatrix}$$

where $\eta = [\eta_1, \cdots, \eta_{n-p}]^T$ and Q is a constant $(n - p) \times n$ matrix which, for the sake of simplicity, is chosen such that each row of Q has only one nonzero term equal to one and the determinant of the $n \times n$ matrix

$$\begin{bmatrix} Q \\ \dfrac{\partial h(x)}{\partial x} \end{bmatrix}$$

is locally nonzero. Here $\partial h(x)/\partial x$ is a $p \times n$ matrix whose ijth entry is $\partial h_i(x)/\partial x_j$. The new variables $\eta_1, , \cdots, , \eta_{n-q}$ are simply $(n - p)$ state variables of the original model of Eq. 1, that satisfy the preceeding determinant condition.

Using the state transformation described earlier, the model of Eq. 1 can be recast in terms of the new state variables η and y:

$$\begin{aligned} \dot{\eta}(t) &= F_\eta[\eta(t), y(t), u(t)] \\ \dot{y}(t) &= F_y[\eta(t), y(t), u(t)] \\ Y_i(t_{ib}) &= \mathfrak{K}_i[\eta(t_{ib} - \theta_i), y(t_{ib} - \theta_i)] \\ & \qquad i = 1, \cdots, q; \quad b = 1, 2, \cdots, \end{aligned} \tag{2}$$

where

$$\begin{aligned} F_\eta[\eta, y, u] &= Qf[\mathfrak{I}^{-1}(\eta, y), u] \\ F_y[\eta, y, u] &= \frac{\partial h(x)}{\partial x} f(x, u)\bigg|_{x = \mathfrak{I}^{-1}(\eta, y)} \\ \mathfrak{K}(\eta, y) &= H[\mathfrak{I}^{-1}(\eta, y)] \end{aligned}$$

We then design a multirate, reduced-order, nonlinear state estimator of the form

$$\begin{aligned} \dot{\xi} &= F_\eta[\xi + Ky, y, u] - KF_y[\xi + Ky, y, u] \\ &\quad + L_p\{Y^* - \mathfrak{K}[\xi + Ky, y]\} + L_I \epsilon \\ \dot{\epsilon} &= Y^* - \mathfrak{K}[\xi + Ky, y] \\ \hat{x} &= \mathfrak{I}^{-1}[\xi + Ky, y] \end{aligned}$$

where $\hat{x}$ is the vector of robustly estimated state variables, ϵ represents the integral of the error between Y^* and its estimate, and Y^* is the *predicted* present value of the vector of the slow measurements. Each component of Y^*, say, Y_i^*, is obtained by a least-squared-error curve fit of a polynomial of order m_i to the most recent r_i measurements of the slow measurable output Y_i, where m_i is chosen such that $r_i > m_i$. The values of r_i and m_i are set by the designer. The state estimator gains K, L_p, and L_I are constant $(n - p) \times p$, $(n - p) \times q$, and $(n - p) \times q$ matrices, respectively. K is the proportional gain with respect to the fast measurements, L_p is the proportional gain with respect to the slow measurements, and L_I is the integral gain with respect to the slow measurements.

Remark 1. As the order of the curve-fitting polynomial, m_i, is increased, the sensitivity of the state estimates to noise in the slow measurements, Y_i, increases. In addition to this, as m_i is increased, more computational power is required to fit a higher-order polynomial. In this article, for every i we set $r_i = 3$ and $m_i = 1$, which are satisfactory for the cases studied here.

The state estimator should be tuned (that is, the constant matrices K, L_p, and L_i should be chosen) such that under nominal conditions, the mismatch between the actual and estimated values of every state variable decays to zero asymptotically. The estimator should be tuned such that the equilibrium point of the error dynamics of the state estimator is asymptotically stable. Assumptions A2 and A3 guarantee the existence of matrices K, L_p, and L_i, such that the eigenval-

ues of the Jacobian matrix of the error dynamics lie in the left half-plane.

The estimator design provides the designer with enough flexibility to set arbitrarily the extent to which the estimates rely on the slow and fast measurements. The gain K represents the weight on the fast measurements, while the gains L_p and L_I represent the proportional and integral weights on the slow measurements, respectively. The gain L_I provides the designer with the ability to add integral action to the estimator. The integral action allows one to obtain more accurate estimates in the presence of model–plant mismatch. In the case where $K = 0$, the estimator relies solely on the slow measurement feedback to obtain the estimates of the states. The reduced-order nature of the estimator also helps reduce the computational time required for estimation.

Reactor System

Figure 1 shows the solution, styrene, free-radical polymerization reactor in DuPont's Marshall Laboratory, Philadelphia, PA. A one-liter glass reactor with baffles was used for the continuous solution polymerization. Toluene was used as solvent and azo-bis-*iso*-butyronitrile (AIBN) as initiator. Two feed tanks were used. One feed tank was filled with a mixture of monomer and solvent, and the other was filled with a mixture of initiator and solvent. From the tanks, the solutions were fed to the reactor at constant flow rates by using two metering pumps. Polymerization reactions were performed under pressure of 20 psia to prevent boiling of the solvent at polymerization temperatures above 100°C. Nitrogen gas was used to maintain pressure in the reactor and to purge oxygen, a known reaction inhibitor, from the reactor. The reaction contents were constantly stirred at approximately 250 rpm during the experiments. The stirrer consisted of two turbines —a three-blade open straight-blade turbine and a four-blade 45°-blade turbine—mounted on a central shaft. A coiled heater in the mantle, in close contact with the reactor, supplied heat to the reactor. A tube surrounding the reactor with holes on the inner curve of the tube was used to blow nitrogen on the reactor when cooling was required. This method of cooling was found to be quite effective. The user interface on a Windows NT operating system was developed using CamileTG data-acquisition and control software (Argonaut Technologies Systems, Inc.).

The reactor temperature was controlled by a proportional-integral (PI) controller. One could set the reactor temperature set point in the user interface. A resistance temperature detector (RTD) was used through a fitting in a port in the reactor to measure the reactor content temperature. The output of the controller caused the output from the heater to vary between 0 and 100%. When the output from the controller ranges from 0 to 50%, the heater output ranges from 0 to 50% and the reactor is cooled simultaneously by blowing nitrogen on the reactor surface. When the output from the controller ranges from 50% to 100%, the heater output varies between 50 and 100%, but there is no simultaneous cooling by blowing nitrogen. Another RTD was introduced in the gap between the reactor and the mantle, and was used to measure the mantle temperature. It allowed one to set the maximum mantle temperature through the computer interface. This greatly helped in reducing the oscillations in the reactor temperature during the runs. Reactor temperature could be controlled within a range of ± 1°C with this control strategy.

Nitrogen gas was continuously injected over the reaction mixture to maintain pressure in the reactor. The reactor pressure was maintained at a constant desired level by a PI controller, which used the degree of vent opening for control. The output of this controller (0–100%) was split-ranged, with the vent opening ranging from 0% to 50% with no nitrogen blown into the reactor, as the controller output ranges from

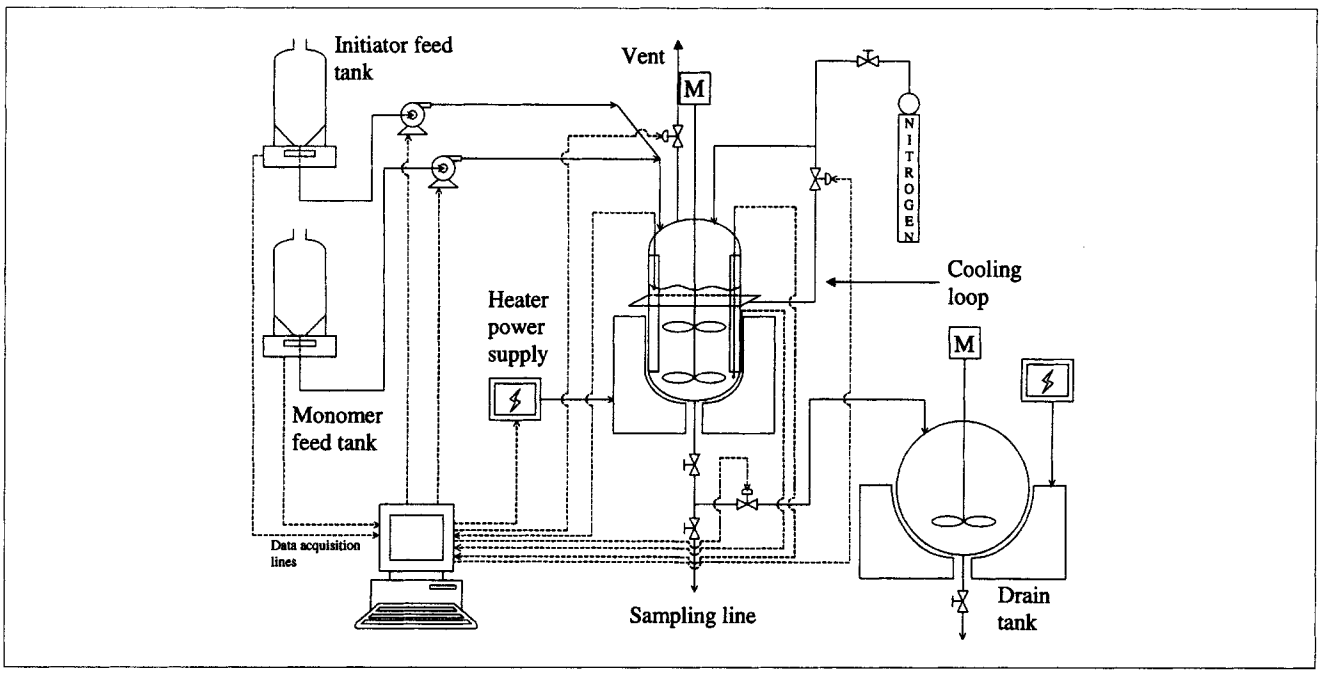

Figure 1. Styrene polymerization reactor setup.

0% to 50%, and with vent opening ranging from 50% to 100% with nitrogen blown into the reactor as the controller output ranges from 50% to 100% to avoid a sudden drop in the reactor pressure.

The feed tanks were placed on two Mettler electronic balances that communicated the changing weight of the tanks to the computer. One could set setpoints for each feed flow rate. A PI controller varied the metering pump output (0–100%) to keep up with the scheduled weight of the feed tanks at any given instant. A very close control on the feed rate was possible using this strategy.

Level control in the reactor was achieved by using another PI controller. An RTD was introduced in the reactor through another fitting in another port. This RTD was placed in a way that the tip just touched the reaction mixture when the reactor was full to the desired level. The computer read the temperature from this RTD as well as the temperature of the reactor contents through another RTD. When the temperature read from the level RTD was less than that of the reactor contents by less than one degree Celsius, the control valve in the drain line was opened for one second. The quantity drained from the reactor every time this happened depended on the degree to which the drain valve (manual) was open. It was advisable to keep the drain valve open to a very small degree to maintain good level control. Another manual valve below the drain valve served to take samples from the reactor periodically. The drained reactor contents accumulated in another glass reactor with 1-gal capacity, which was also continuously stirred. Periodically, the contents of this drain reactor were emptied into a kill solution (1% benzoquinone).

Offline measurements

Measurements obtained via offline analysis were used online with a time-delay corresponding to the analysis time. One-ounce sample bottles filled with 25 g of inhibitor solution (0.1% methyl hydroquinone in toluene) were kept ready in dry ice. Samples were withdrawn from the reactor every hour from the manual drain valve at the bottom of the reactor. As soon as the sample was collected, 25 g of the sample was added to the cold sample bottles to quench the reaction immediately.

One vial was loaded with the sample solution from the sample bottle for a styrene concentration measurement using a Hewlett-Packard (Palo Alto, CA) gas chromatograph (GC), model 6890. No dilution of the sample was required for the GC measurement, because the sample was already very dilute due to high solvent concentration as well as 50% inhibitor solution by weight. Another vial was filled with the sample solution after diluting it 25 times for molecular-weight distribution measurements using a gel permeation chromatograph (GPC), a Hewlett-Packard model 1050 gradient liquid chromatograph. Tetrahydrofuran (THF) was used to dilute the sample. The sample vials were then taken to the analytical lab for analysis. The GC and GPC were linked to the main server. Hence, the data from these instruments could be analyzed directly on the lab computer. The GC and GPC measurements were obtained in approximately 45 min. A simple standard procedure was followed to get the solids concentration in the sample via gravimetric analysis. The procedure took approximately 50 min. Styrene concentration could then be back-calculated from the solids measurements by using the known styrene concentration in the feed.

Mathematical Model

The performance of an estimator obviously depends highly on the accuracy of the process model. Hence, the main concern in model development was that it should be able to at least predict the trends in the process variables due to changes in any process inputs. The final model was a modification of the model presented inTatiraju and Soroush (1997), so that it met our experimental operating conditions. This modification involved some changes in mass balance equations. Moreover, the equations for the zeroth and second moments (λ_0, λ_2) of dead-polymer molecular-weight distribution were replaced by number-average molecular weight (M_n) and weight-average molecular weight (M_w) of the dead-polymer chains. This was done so that the available infrequent measurements of average molecular weights could be used directly in the estimator design. The model has the form

$$\frac{dC_i}{dt} = -\left[\frac{F_t}{V} + k_i\right]C_i + \frac{F_i C_{i_i}}{V}$$

$$\frac{dC_s}{dt} = -\frac{F_t C_s}{V} + \frac{F_i C_{s_i} + F_m C_{s_m}}{V}$$

$$\frac{dM_n}{dt} = f_3(M_n, C_i, C_s, C_m, T)$$

$$\frac{d\lambda_1}{dt} = -\frac{F_t \lambda_1}{V} + f_4(C_i, C_s, C_m, T)$$

$$\frac{dM_w}{dt} = f_5(M_w, C_i, C_s, C_m, T)$$

$$\frac{dC_m}{dt} = f_6(C_i, C_m, T) + \frac{F_m C_{m_m} - F_t C_m}{V} \tag{3}$$

where

$$f_3(M_n, C_i, C_s, C_m, T) = \left\{\left[\left(k_{f_m}C_m + k_{t_d}P + k_{f_s}C_s\right)(2\alpha - \alpha^2) + k_{t_c}P\right]M_m - \left[\left(k_{f_m}C_m + k_{t_d}P + k_{f_s}C_s\right)\alpha + 0.5k_{t_c}P\right]M_n(1-\alpha)\right\}\frac{PM_n}{\lambda_1(1-\alpha)}$$

$$f_4(C_i, C_s, C_m, T) = \left[\left(k_{f_m}C_m + k_{t_d}P + k_{f_s}C_s\right)(2\alpha - \alpha^2) + k_{t_c}P\right]\frac{PM_m}{(1-\alpha)}$$

$$f_5(M_w, C_i, C_s, C_m, T) = \left\{\left[\left(k_{f_m}C_m + k_{t_d}P + k_{f_s}C_s\right)(\alpha^3 - 3\alpha^2 + 4\alpha) + k_{t_c}P(\alpha + 2)\right]M_m - \left[\left(k_{f_m}C_m + k_{t_d}P + k_{f_s}C_s\right)(2\alpha - \alpha^2) + k_{t_c}P\right]M_w(1-\alpha)\right\}\frac{PM_m}{\lambda_1(1-\alpha)^2}$$

Table 1. Model Parameter Values

$A_i = 7.142\times10^3$	K	VAZO Product Bulletin, DuPont
$B_i = -1.836\times10^1$		VAZO Product Bulletin, DuPont
$A_{f_m} = 2.310\times10^6$	$m^3\cdot kmol^{-1}\cdot s^{-1}$	Schmidt and Ray, 1981
$E_{f_m}/R = 6.377\times10^3$	K	Schmidt and Ray, 1981
$A_p = 9.500\times10^6$	$m^3\cdot kmol^{-1}\cdot s^{-1}$	This work
$E_p/R = 3.600\times10^3$	K	This work
$A_t = 1.250\times10^9$	$m^3\cdot kmol^{-1}\cdot s^{-1}$	Schmidt and Ray, 1981
$E_t/R = 8.430\times10^2$	K	Schmidt and Ray, 1981
$k_{t_d} = 0.15\times k_t$	$m^3\cdot kmol^{-1}\cdot s^{-1}$	This work
$k_{t_c} = 0.85\times k_t$	$m^3\cdot kmol^{-1}\cdot s^{-1}$	This work
$A_{f_s} = 9.950\times10^{10}$	$m^3\cdot kmol^{-1}\cdot s^{-1}$	Schmidt and Ray, 1981
$E_{f_s}/R = 1.100\times10^4$	K	Schmidt and Ray, 1981
$f^* = 6.300\times10^{-1}$		This work
$M_m = 1.040\times10^2$	$kg\cdot kmol^{-1}$	

$$f_6(C_i, C_m, T) = -k_p C_m P$$

$$\alpha = \frac{k_p C_m}{(k_p + k_{f_m})C_m + k_{f_s}C_s + k_t P}$$

$$P = \sqrt{\frac{2f^* C_i k_i}{k_t}}$$

The energy balance equations were omitted from the model because temperature in the reactor was measured and fed to the estimator frequently online.

The parameter values used in the model are summarized in Table 1. Under the operating conditions of the reactor given in Table 2 and the high solvent fraction in the feed, the gel and glass effects were negligible (Schmidt and Ray, 1981). Hence, it was not necessary to include those effects in the process model.

Parameter Estimation and Model Validation

The model presented in the previous section could not predict the preliminary experimental data satisfactorily. Hence, it was necessary to improve the model predictions by estimating some of the model parameters. For this purpose, optimization simulations were carried out to reduce the least-squared error between the model predictions and the available experimental values of polymer weight-average and number-average molecular weights, and monomer concentration. These optimization simulations led to changes in the values of the parameters, initiator efficiency, f^*, Arrhenius constant and activation energy related to the propagation step, A_p and E_p, and the ratio of termination by combination reaction-rate constant to termination by disproportionation reaction-rate constant, $r_{c/d}$. The new values obtained for these parameters are

$$f^* = 0.63; \quad A_p = 9.5\times10^6\ m^3\cdot kmol^{-1}\cdot s^{-1};$$

$$E_p/R = 3{,}600\ K; \quad r_{c/d} = 85/15$$

These values are different from those available in the literature (Schmidt and Ray, 1981) by less than 10%. Furthermore, the following initiation-rate constant was used

$$k_i = 0.693/[60\times10^{((A_i/T)+B_i)}]$$

where the values of A_i and B_i are given in Table 1 to improve the M_w and M_n prediction accuracy of the model. This initiation-rate constant was obtained from DuPont's prior research studies (*VAZO Product Bulletin*, 1989).

Many polymerization experiments were then performed for model validation. Each experiment included many changes like temperature change, initiator flow-rate change, and monomer flow-rate change, to assure adequate accuracy of the model predictions in the entire operating range of interest. The temperature and flow rate measurements were procured by the data-acquisition software every second and recorded in a log file to be used for offline simulations later. When required, a sample was withdrawn for off-line measurements of monomer concentration and molecular-weight distribution. However, these infrequent measurements were available all together after each experiment was complete.

Figures 2, 3, and 4 compare the final-model predictions of M_w, M_n, and monomer concentration (C_m) with actual measurements from a typical model validation experiment. Table 3 summarizes the series of changes in the operating conditions during the course of this experiment. The continuous line represents the model predictions, whereas the bullets represent the infrequent and delayed measurements. Error bars represent 5% error in the measurements. As can clearly be seen, the model is accurate enough to predict the trend in all the measurements, with the changes in process operating conditions, perfectly. However, there is slight mismatch between the model predictions and the experimental data dur-

Table 2. Operating Conditions of the Polymerization Reactor

$C_m(0) = 0.000\times10^0$	$kmol\cdot m^{-3}$
$C_i(0) = 0.000\times10^0$	$kmol\cdot m^{-3}$
$C_s(0) = 9.391\times10^0$	$kmol\cdot m^{-3}$
$T(0) = 3.930\times10^2$	K
$C_{m_m} = 7.208\times10^0$	$kmol\cdot m^{-3}$
$C_{i_i} = 1.138\times10^{-1}$	$kmol\cdot m^{-3}$
$C_{s_i} = 9.200\times10^0$	$kmol\cdot m^{-3}$
$C_{s_m} = 1.750\times10^0$	$kmol\cdot m^{-3}$
$V = 4.8\times10^{-4}$	m^3 (model validation experiment)
$V = 4.5\times10^{-4}$	m^3 (estimation experiment)

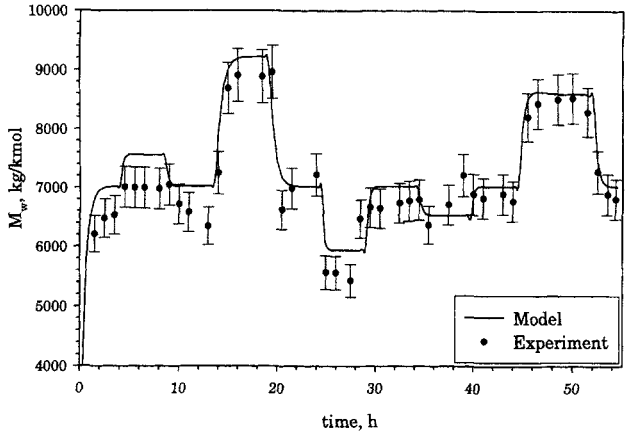

Figure 2. Weight-average molecular weight vs. time for the model validation experiment:—, model prediction; ●, offline measurements.

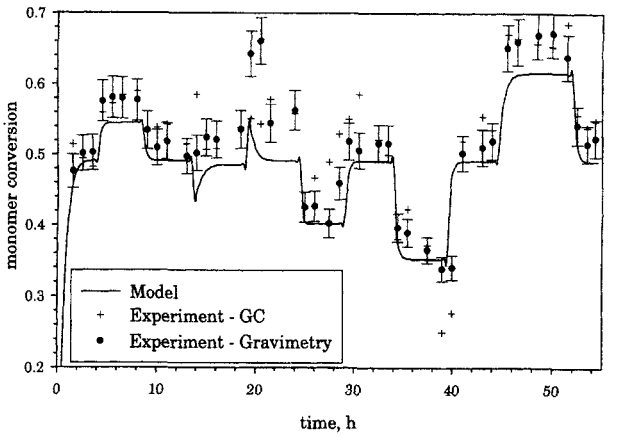

Figure 4. Monomer conversion vs. time for the model validation experiment:—, model prediction; ●, off-line gravimetric measurements; +, offline GC measurements.

ing some time periods. This may be due to some unknown disturbances in the process, such as a slight change in feed concentration, reactor temperature, or the like.

The general understanding in free-radical polymerization is that a higher temperature leads to reduced average molecular weight. For styrene, average molecular weight drops with temperatures up to about 120°C, after which it increases slightly. The drop with temperature early on is owing to the further conversion of initiator to nearly 100%. As the initiator nears 100%, the increasing monomer conversion serves to increase the resulting molecular weight.

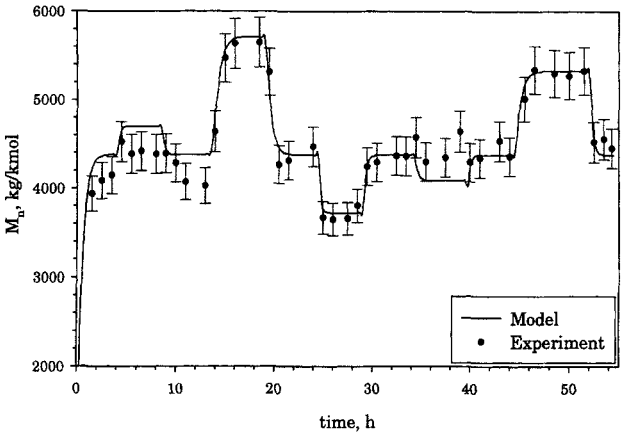

Figure 3. Number-average molecular weight vs. time for the model validation experiment:—, model prediction; ●, offline measurements.

The monomer concentration measurements obtained via GC (represented by plus signs in the graph) and via gravimetric analysis (represented by dots in the graph) were strikingly different. The gravimetric data displayed consistent trends in the measurements, whereas the GC measurements displayed a lot of noise. This was observed in all the model validation results. A reason for this can be wrong calibration of the GC instrument. Due to this observation, it was decided to use gravimetric data for online estimation experiments. GC was still used for monomer concentration measurements during the online experiments, but the data from GC served as only a rough check on the gravimetric measurements.

Robust Multirate State Estimator

The application of the state estimation method, described in the second section, to this polymerization reactor led to

Table 3. Changes in the Operating Conditions of the Reactor During the Model Validation Experiment

Time, (h)	Change in the Operating Conditions		
0.0	$T = 393$ K,	$F_i = 1.5414 \times 10^{-4}$ m^3/s,	$F_m = 1.5414 \times 10^{-4}$ m^3/s
4.0	$T = 403$ K,	$F_i = 1.5414 \times 10^{-4}$ m^3/s,	$F_m = 1.5414 \times 10^{-4}$ m^3/s
8.5	$T = 393$ K,	$F_i = 1.5414 \times 10^{-4}$ m^3/s,	$F_m = 1.5414 \times 10^{-4}$ m^3/s
13.5	$T = 393$ K,	$F_i = 1.156 \times 10^{-4}$ m^3/s,	$F_m = 1.5414 \times 10^{-4}$ m^3/s
19.0	$T = 393$ K,	$F_i = 1.5414 \times 10^{-4}$ m^3/s,	$F_m = 1.5414 \times 10^{-4}$ m^3/s
24.5	$T = 393$ K,	$F_i = 3.0828 \times 10^{-4}$ m^3/s,	$F_m = 3.0828 \times 10^{-4}$ m^3/s
29.0	$T = 393$ K,	$F_i = 1.5414 \times 10^{-4}$ m^3/s,	$F_m = 1.5414 \times 10^{-4}$ m^3/s
34.0	$T = 373$ K,	$F_i = 1.5414 \times 10^{-4}$ m^3/s,	$F_m = 1.5414 \times 10^{-4}$ m^3/s
39.5	$T = 393$ K,	$F_i = 1.5414 \times 10^{-4}$ m^3/s,	$F_m = 1.5414 \times 10^{-4}$ m^3/s
44.5	$T = 393$ K,	$F_i = 9.6338 \times 10^{-3}$ m^3/s,	$F_m = 9.6338 \times 10^{-3}$ m^3/s
52.0	$T = 393$ K,	$F_i = 1.5414 \times 10^{-4}$ m^3/s,	$F_m = 1.5414 \times 10^{-4}$ m^3/s

the robust, multirate, nonlinear state estimator

$$\begin{bmatrix} \frac{d\hat{C}_i}{dt} \\ \frac{d\hat{C}_s}{dt} \\ \frac{d\hat{M}_n}{dt} \\ \frac{d\hat{\lambda}_1}{dt} \\ \frac{d\hat{M}_w}{dt} \\ \frac{d\hat{C}_m}{dt} \\ \frac{d\epsilon_1}{dt} \\ \frac{d\epsilon_2}{dt} \\ \frac{d\epsilon_3}{dt} \end{bmatrix} = \begin{bmatrix} -\left[\frac{F_t}{V}+k_i\right]\hat{C}_i + \frac{F_i C_{i_i}}{V} \\ -\frac{F_t\hat{C}_s}{V} + \frac{F_i C_{s_i} + F_m C_{s_m}}{V} \\ f_3\left(\hat{M}_n, \hat{C}_i, \hat{C}_s, \hat{\lambda}_1, \hat{C}_m, T\right) \\ -\frac{F_t\hat{\lambda}_1}{V} + f_4\left(\hat{C}_i, \hat{C}_s, \hat{C}_m, T\right) \\ f_5\left(\hat{M}_w, \hat{C}_i, \hat{C}_s, \hat{\lambda}_1, \hat{C}_m, T\right) \\ \frac{F_m C_{m_m} - F_t\hat{C}_m}{V} + f_6\left(\hat{C}_i, \hat{C}_m, T\right) \\ 0 \\ 0 \\ 0 \end{bmatrix} + \begin{bmatrix} L_p \\ I_3 \end{bmatrix} \begin{bmatrix} M_n^* - \hat{M}_n \\ M_w^* - \hat{M}_w \\ C_m^* - \hat{C}_m \end{bmatrix} + \begin{bmatrix} L_I \\ 0_3 \end{bmatrix} \begin{bmatrix} \epsilon_1 \\ \epsilon_2 \\ \epsilon_3 \end{bmatrix} \tag{4}$$

where $L_p = [L_{p_{ij}}]$ and $L_I = [L_{I_{ij}}]$ are the estimator gains, 0_n and I_n represent a nth-order null matrix and unity matrix, respectively, and $M_n^*(t)$, $M_w^*(t)$, and $C_m^*(t)$ are the predicted present values of the infrequent measurable outputs, each of which was obtained by fitting a least-squared-error line to the most recent three measurements of M_w, M_n, and C_m, respectively. However, at startup, the predicted present values were obtained by fitting a straight line to the first two measurements as soon as they were available. The initial estimator conditions, given in Table 4, were chosen to match the initial experimental conditions.

The online implementation of the estimator consisted of two software interfaces developed using CamileTG PC data-acquisition and control software. The first interface (experimental interface) handled all the control and data acquisition, which were directly related to the process. This interface made it very easy to set all the operating conditions for the reactor from the computer. The estimator equations were implemented in the second interface (estimator interface). The fourth-order Runge–Kutta fixed-step numerical integration algorithm with a step size of 1 s was used to integrate the model equations numerically. The estimator interface could directly access the temperature and flow-rate measurements from the experimental interface. The estimator interface had text boxes to feed in the infrequent measurements whenever they were available. All the estimated state variables could be plotted during the experiment along with the measurements, thus making it possible to monitor the performance of the estimator at any given point of time. Furthermore, the software logged all the experimental data during the runs. These logged data can then be used to rerun any particular experiment under a simulation mode. This feature makes it very easy to fine-tune the estimator offline.

Table 4. Initial Conditions of the Estimator

$\hat{C}_m(0) = 0.000\times10^{0}$	$\text{kmol}\cdot\text{m}^{-3}$
$\hat{C}_i(0) = 1.000\times10^{-8}$	$\text{kmol}\cdot\text{m}^{-3}$
$\hat{C}_s(0) = 9.391\times10^{0}$	$\text{kmol}\cdot\text{m}^{-3}$
$\hat{M}_n(0) = 2.000\times10^{2}$	$\text{kmol}\cdot\text{m}^{-3}$
$\hat{\lambda}_1(0) = 1.000\times10^{-3}$	$\text{kg}\cdot\text{m}^{-3}$
$\hat{M}_w(0) = 2.000\times10^{2}$	$\text{kg}^2\cdot\text{kmol}^{-1}\cdot\text{m}^{-3}$

Estimator tuning

Since, by using M_w, M_n, and C_m measurements, the only states that could be estimated robustly are M_w, M_n, and C_m themselves, all components of the gain matrices L_p and L_I, except for $L_{p_{31}}$, $L_{p_{52}}$, $L_{p_{63}}$, $L_{I_{31}}$, $L_{I_{52}}$, and $L_{I_{63}}$ were set to zero. The nonzero gains of the estimator needed to be selected such that the estimator error dynamics given by

$$\begin{aligned}
\dot{e}_1 &= -\left[k_i + \frac{1}{\tau}\right]e_1 \\
\dot{e}_2 &= -\frac{1}{\tau}e_2 \\
\dot{e}_6 &= -\frac{1}{\tau}e_6 + \Delta f_6(e_1, e_6, C_i, C_m, T) \\
&\qquad - L_{p_{63}}e_6 + L_{p_{63}}(C_m^* - C_m)L_{I_{63}}\epsilon_3 \\
\dot{\epsilon}_3 &= -e_6 + (C_m^* - C_m) \\
\dot{e}_4 &= -\frac{1}{\epsilon}e_4 + \Delta f_4(e_1, e_2, e_6, C_i, C_s, C_m, T) \\
\dot{e}_3 &= \Delta f_3(e_1, e_2, e_3, e_4, e_6, C_i, C_s, M_n, \lambda_1, C_m, T) \\
&\qquad - L_{p_{31}}e_3 + L_{p_{31}}(M_n^* - M_n) + L_{I_{31}}\epsilon_1 \\
\dot{\epsilon}_1 &= -e_3 + (M_n^* - M_n) \\
\dot{e}_5 &= \Delta f_5(e_1, e_2, e_4, e_5, e_6, C_i, C_s, M_w, \lambda_1, C_m, T) \\
&\qquad - L_{p_{52}}e_5 + L_{p_{52}}(M_w^* - M_w) + L_{I_{52}}\epsilon_2 \\
\dot{\epsilon}_2 &= -e_5 + (M_w^* - M_w)
\end{aligned} \tag{5}$$

where

$$\begin{aligned}
&\Delta f_3(e_1, e_2, e_3, e_4, e_6, C_i, C_s, M_n, \lambda_1, C_m, T) \\
&\quad = f_3(C_i + e_1, C_s + e_2, M_n + e_3, \lambda_1 + e_4, C_m + e_6, T) \\
&\qquad - f_3(C_i, C_s, M_n, \lambda_1, C_m, T) \\
&\Delta f_4(e_1, e_2, e_6, C_i, C_s, C_m, T) \\
&\quad = f_4(C_i + e_1, C_s + e_2, C_m + e_6, T) - f_4(C_i, C_s, C_m, T) \\
&\Delta f_5(e_1, e_2, e_4, e_5, e_6, C_i, C_s, M_w, \lambda_1, C_m, T) \\
&\quad = f_5(C_i + e_1, C_s + e_2, M_w + e_5, \lambda_1 + e_4, C_m + e_6, T) \\
&\qquad - f_5(C_i, C_s, M_w, \lambda_1, C_m, T) \\
&\Delta f_6(e_1, e_6, C_i, C_m, T) \\
&\qquad = f_6(C_i + e_1, C_m + e_6, T) - f_6(C_i, C_m, T)
\end{aligned}$$

were locally asymptotically stable. This was achieved by placing all eigenvalues of the Jacobian of the system of Eq. 5

$$J=\begin{bmatrix} -\left(k_i+\frac{1}{\tau}\right) & 0 & 0 & 0 & 0 & 0 & 0 & 0 \\ 0 & -\frac{1}{\tau} & 0 & 0 & 0 & 0 & 0 & 0 \\ J_{61} & 0 & J_{66} & L_{I_{63}} & 0 & 0 & 0 & 0 \\ 0 & 0 & -1 & 0 & 0 & 0 & 0 & 0 \\ J_{41} & J_{42} & J_{46} & 0 & -\frac{1}{\tau} & 0 & 0 & 0 \\ J_{31} & J_{32} & J_{36} & 0 & J_{34} & J_{33} & L_{I_{31}} & 0 \\ 0 & 0 & 0 & 0 & 0 & -1 & 0 & 0 \\ J_{51} & J_{52} & J_{56} & 0 & J_{54} & 0 & 0 & J_{55} \\ 0 & 0 & 0 & 0 & 0 & 0 & 0 & -1 \end{bmatrix} \quad \begin{matrix} 0 \\ 0 \\ L_{I_{52}} \\ 0 \end{matrix}$$

in the left half-plane. Since the preceding Jacobian is a lower block-triangular matrix, its nine eigenvalues are

$$\lambda_1': -\left(k_i+\frac{1}{\tau}\right)$$

$$\lambda_2': -\frac{1}{\tau}$$

$$\lambda_3', \lambda_4': \text{roots of } \left(\lambda^2 - J_{66}\lambda + L_{I_{63}}\right)$$

$$\lambda_5': -\frac{1}{\tau}$$

$$\lambda_6', \lambda_7': \text{roots of } \left(\lambda^2 - J_{33}\lambda + L_{I_{31}}\right)$$

$$\lambda_8', \lambda_9': \text{roots of } \left(\lambda^2 - J_{55}\lambda - L_{I_{52}}\right),$$

where

$$J_{66}=\left.\frac{\partial f_6}{\partial C_m}\right|_{ss} - \frac{1}{\tau} - L_{p_{63}}$$

$$J_{33}=\left.\frac{\partial f_3}{\partial M_n}\right|_{ss} - L_{p_{31}}$$

$$J_{55}=\left.\frac{\partial f_5}{\partial M_w}\right|_{ss} - L_{p_{52}}$$

The eigenvalues λ_1', λ_2', and λ_5' are inherently negative (since k_i and τ are always positive), and hence the rate of convergence of the estimates of initiator concentration, solvent concentration, and first moment of MWD cannot be set by the designer, but are set by the process itself. The other six eigenvalues will also have negative real parts, if the gain components are set such that

$$J_{66} \le 0, \quad J_{33} \le 0, \quad J_{55} \le 0$$

$$L_{I_{63}} \ge 0, \quad L_{I_{31}} \ge 0, \quad L_{I_{52}} \ge 0.$$

It can be easily verified that the terms

$$\left.\frac{\partial f_6}{\partial C_m}\right|_{ss}, \quad \left.\frac{\partial f_3}{\partial M_n}\right|_{ss}, \quad \left.\frac{\partial f_5}{\partial M_w}\right|_{ss}$$

are negative under all conditions. Hence, all positive values of the proportional gains will guarantee stable estimator error dynamics

$$L_{p_{63}} \ge 0, \quad L_{p_{31}} \ge 0, \quad L_{p_{52}} \ge 0$$

Furthermore, the higher the values of the L_p gains, the faster is the decay of the corresponding estimator errors. However, this may increase the sensitivity of the estimates of the corresponding state variables to the infrequent measurements, which is not advisable if the infrequent measurements are accompanied by noise. The higher the values of the L_I gains, the more are the oscillations in the estimator response (since this will increase the imaginary part of the eigenvalues λ_3', λ_4', λ_6', ..., λ_9'). To avoid any oscillation in the estimator performance, it was necessary to impose further restrictions on the gains. Those are

$$J_{66}^2 - 4L_{I_{63}} \ge 0$$

$$J_{33}^2 - 4L_{I_{31}} \ge 0$$

$$J_{55}^2 - 4L_{I_{52}} \ge 0$$

The selection of the observer gains according to the aforementioned conditions ensures asymptotic stability of the observer error dynamics. The observer gains can be fine-tuned further for required performance via simulations. The gain values used for all the estimation experiments concerned with this article are given in Table 5.

Estimation Results

Several online experiments were performed to test the performance of the estimator. Each experiment involved a series of operating condition changes to assure the excellent perfor-

Table 5. Nonzero Gain Values of the Estimator

Gain	Value
$L_{p_{31}} =$	5.0×10^{-5}
$L_{p_{52}} =$	5.0×10^{-5}
$L_{p_{63}} =$	5.0×10^{-5}
$L_{I_{31}} =$	5.0×10^{-8}
$L_{I_{52}} =$	5.0×10^{-8}
$L_{I_{63}} =$	5.0×10^{-8}

mance of the estimator. Measurements of M_w, M_n, and C_m were obtained infrequently at every hour, with a time delay of approximately 1 h. These measurements were fed to the estimator online through the experimental interface when they were available.

This section presents a representative set of results for one of the experiments. Table 6 summarizes the series of changes in the operating conditions during the course of this estimation experiment. Figures 5, 6, and 7 show the estimation results in the form of plots of M_w, M_n, and C_m, respectively, vs. time. The continuous line represents the estimates, and the bullets represent the infrequent and delayed experimental measurements obtained offline. Error bars represent 5% error in the measurements. In the graphs, the measurements are shown at the time when the sample was withdrawn. However, these measurements were used in estimation when they were actually available from the analytical lab (approximately 45–55 min after sampling).

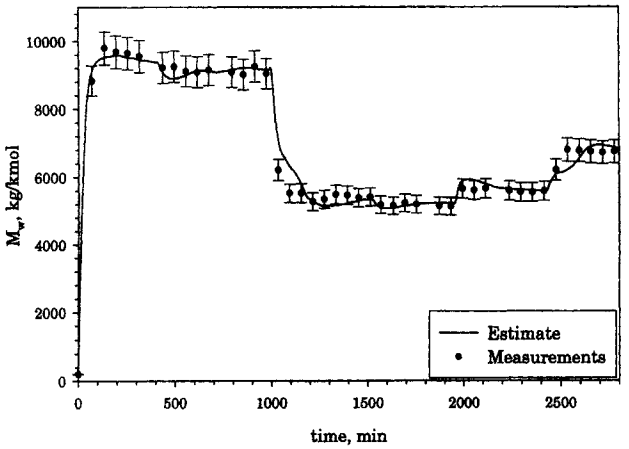

Figure 5. Weight-average molecular weight vs. time for the online estimation experiment:—, estimate; ●, offline measurements.

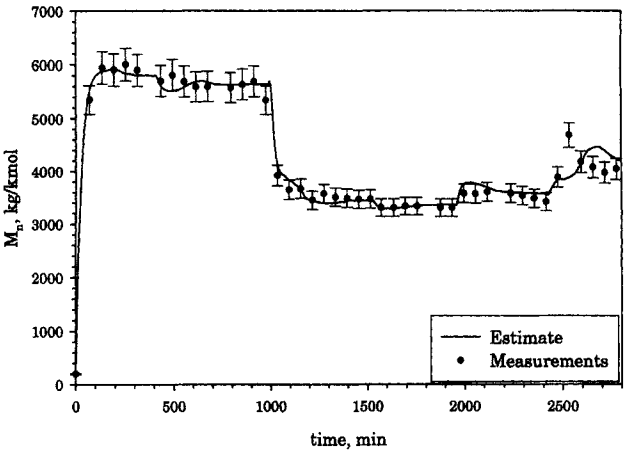

Figure 6. Number-average molecular weight vs. time for the online estimation experiment:—, estimate; ●, offline measurements.

As shown in Figures 5, 6, and 7, the estimator was able to accurately calculate frequent estimates of all of three states by using their infrequent and delayed measurements. In the C_m plot, initially there was a significant error between the measurements and the estimates. However, in about 5–6 h, the estimator was able to completely eliminate this error, giving accurate estimates thereafter. Furthermore, the estimator

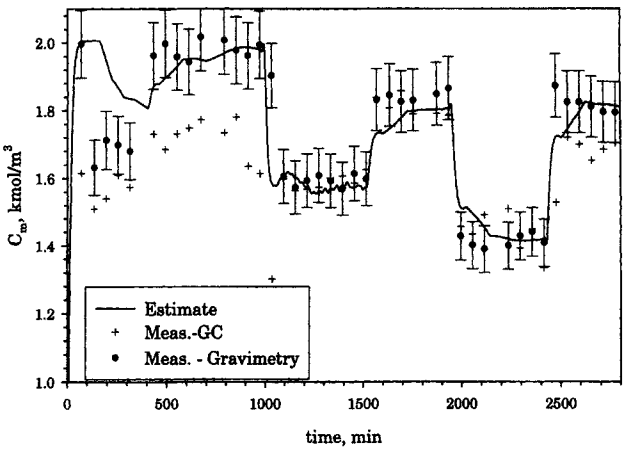

Figure 7. Monomer concentration vs. time for the online estimation experiment:—, estimate; ●, offline gravimetric measurements; +, offline GC measurements.

Table 6. Changes in the Operating Conditions During the Course of the Estimation Experiment

Time, (h)	Change in the Operating Conditions		
0.0	$T = 403$ K,	$F_i = 1.156\times10^{-4}$ m^3/s,	$F_m = 1.5414\times10^{-4}$ m^3/s
400	$T = 393$ K,	$F_i = 1.156\times10^{-4}$ m^3/s,	$F_m = 1.5414\times10^{-4}$ m^3/s
1,000	$T = 393$ K,	$F_i = 1.9268\times10^{-4}$ m^3/s,	$F_m = 1.5414\times10^{-4}$ m^3/s
1,520	$T = 383$ K,	$F_i = 1.9268\times10^{-4}$ m^3/s,	$F_m = 1.5414\times10^{-4}$ m^3/s
1,950	$T = 430$ K,	$F_i = 1.9268\times10^{-4}$ m^3/s,	$F_m = 1.5414\times10^{-4}$ m^3/s
2,430	$T = 393$ K,	$F_i = 1.5414\times10^{-4}$ m^3/s,	$F_m = 1.5414\times10^{-4}$ m^3/s

is able to handle several unknown disturbances, such as sudden drop and rise in feed flow-rates, change in the feed concentration, and change in reactor residence time. The accuracy of all the estimates was obvious, because the estimates always lay within the experimental error at all times. Because of the high accuracy of the estimator, the estimates can be successfully used as feedback control to regulate the molecular-weight distribution and conversion in the polymerization reactor considered in this study.

Conclusions

A robust multirate nonlinear state estimator was implemented on a polymerization reactor online. The estimator is applicable to processes with infrequent measurements that are available irregularly; the design and implementation of the estimator for these processes remain the same as in the polymerization case study. Unlike most other estimators, the robust estimator is not case specific, that is, the estimator design is applicable to a variety of processes. The estimator calculated robust frequent estimates of polymer weight-average and number-average molecular weights, and monomer concentration from (1) online frequent measurements of the reactor temperature, and (2) offline, infrequent, and delayed measurements of polymer weight-average and number-average molecular weights, and monomer concentration. The estimator was able to eliminate the initial mismatch between the measurements of monomer concentration and its estimates. During the course of the experiments, the estimator was able to calculate reliable estimates in the presence of several disturbances unknown to the estimator, such as sudden drop and rise in feed flow-rates, change in the feed concentration, and change in reactor residence time. The estimation results showed that the calculated estimates were accurate enough (estimates always lie within error bars of the infrequent measurements) to be used for feedback control.

Acknowledgments

Financial support from the National Science Foundation through Grant CTS-9703278 and DuPont is gratefully acknowledged. The authors thank Babatunde A. Ogunnaike, John P. Congalidis, and John R. Richards for their invaluable insightful comments. The authors also thank Vincent C. Stonis, Shawn P. Malone, John M. Hammell, and Christopher A. Samuel for their invaluable help in performing the experiments, and Timothy A. Kutz for his help in coding the Camile data interface.

Notation

C_i = concentration of initiator in the reactor, kmol·m^{-3}
C_{i_i} = initiator concentration in initiator feed stream, kmol·m^{-3}
$\hat{C}_i$ = estimated value of initiator concentration in the reactor, kmol·m^{-3}
C_m = concentration of monomer in the reactor, kmol·m^{-3}
C_{m_m} = monomer concentration in monomer feed stream, kmol·m^{-3}
$\hat{C}_m$ = estimated value of monomer concentration in the reactor, kmol·m^{-3}
C_m^* = predicted present value of monomer concentration in the reactor, kmol·m^{-3}
C_s = concentration of solvent in the reactor, kmol·m^{-3}
C_{s_i} = solvent concentration in initiator feed stream, kmol·m^{-3}
C_{s_m} = solvent concentration in monomer feed stream, kmol·m^{-3}
$\hat{C}_s$ = estimated value of solvent concentration in the reactor, kmol·m^{-3}
f^* = initiator efficiency
F_i = inlet initiator stream flow rate, m^3·s^{-1}
F_m = inlet monomer stream flow rate, m^3·s^{-1}
$F_t = (F_m + F_i)$, reactor outlet stream flow rate, m^3·s^{-1}
$k_{f_m} = A_{f_m} \exp(-E_{f_m}/T)$, rate constant for chain transfer to monomer reactions, m^3·kmol^{-1}·s^{-1}
$k_{f_s} = A_{f_s} \exp(-E_{f_s}/T)$, rate constant for chain transfer to solvent reactions, m^3·kmol^{-1}·s^{-1}
$k_i = 0.693/[60 \times 10^{((A_i/T)+B_i)}]$, dissociation rate constant for initiator, s^{-1}
$k_p = A_p \exp(-E_p/T)$, rate constant for propagation reactions, m^3·kmol^{-1}·s^{-1}
$k_t = A_t \exp(-E_t/T)$, rate constant for termination reactions, m^3·kmol^{-1}·s^{-1}
k_{t_c} = rate constant for termination via combination reactions, m^3·kmol^{-1}·s^{-1}
k_{t_d} = rate constant for termination via disproportionation reactions, m^3·kmol^{-1}·s^{-1}
L_p = proportional estimator gain
L_I = integral estimator gain
M_n = number-average molecular weight of the polymer, kg·kmol^{-1}
$\hat{M}_n$ = estimated value of number-average molecular weight of the polymer, kg·kmol^{-1}
M_n^* = predicted present value of number-average molecular weight of the polymer, kg·kmol^{-1}
M_w = weight-average molecular weight of the polymer, kg·kmol^{-1}
$\hat{M}_w$ = estimated value of weight-average molecular weight of the polymer, kg·kmol^{-1}
M_w^* = predicted present value of weight-average molecular weight of the polymer, kg·kmol^{-1}
P = molar concentration of live polymer, kg·kmol^{-1}
$r_{c/d} = k_{t_c}/kt_d$
t = time, s
T = temperature of the reactor contents, K
V = reactor volume, m^3

Greek letters

λ_1 = first moment of the MWD, kg·m^{-3}
$\hat{\lambda}_1$ = estimated value of first moment of the MWD, kg·m^{-3}
τ = reactor residence time $[V/(F_i + F_m + F_s)]$, s

Literature Cited

Acuna, G., E. Latrille, C. Beal, and G. Corrieu, "On-Line Estimation of Biological Variables During pH Controlled Lactic Acid Fermentations," *Biotechnol. Bioeng.*, **44**, 1168 (1994).

Bastin, G., and D. Dochain, *Online Estimation and Adaptive Control of Bioreactors*, Elsevier, New York (1990).

Bastin, G., and D. Dochain, "On-Line Estimation of Microbial Specific Growth Rates," *Automatica*, **22**, 705 (1986).

Claes, J. E., and J. F. Van Impe, "On-Line Estimation of the Specific Growth Rate Based on Viable Biomass Measurements: Experimental Validation," *Bioprocess Eng.*, **21**, 389 (1999).

Dochain, D., and A. Pauss, "On-Line Estimation of Microbial Specific Growth-Rates: An Illustrative Case Study," *Can. J. Chem. Eng.*, **66**, 626 (1988).

Elicabe, G. E., E. Ozdeger, C. Georgakis, and C. Cordeiro, "On-Line Estimation of Reaction Rates in Semicontinuous Reactors," *Ind. Eng. Chem. Res.*, **34**, 1219 (1995).

Ellis, M. F., T. W. Taylor, V. Gonzalez, and K. F. Jensen, "Estimation of the Molecular Weight Distribution in Batch Polymerization," *AIChE J.*, **34**, 1341 (1988).

Ellis, M. F., T. W. Taylor, and K. F. Jensen, "On-Line Molecular Weight Distribution Estimation and Control in Batch Polymerization," *AIChE J.*, **40**, 445 (1994).

Embirucu, M., E. L. Lima, and J. C. Pinto, "A Survey of Advanced Control of Polymerization Reactors," *Poly. Eng. Sci.*, **36**, 433 (1996).

Farza, M., H. Hammouri, C. Jallut, and J. Lieto, "State Observation of a Nonlinear System: Application to (Bio)Chemical Processes," *AIChE J.*, **45**, 93 (1999).

Gauthier, J. P., H. Hammouri, and S. Othman, "A Simple Observer for Non-Linear Systems. Application to Bioreactors," *IEEE Trans. Autom. Control*, **AC-37**, 875 (1992).

Gudi, R. D., S. L. Shah, and M. R. Gray, "Multirate State and Parameter Estimation in an Antibiotic Fermentation with Delayed Measurements," *Biotechnol. Bioeng.*, **44**, 1271 (1994).

Gudi, R. D., S. L. Shah, and M. R. Gray, "Adaptive Multirate State and Parameter Estimation Strategies with Application to a Bioreactor," *AIChE J.*, **41**, 2451 (1995).

Gudi, R. D., S. L. Shah, M. R. Gray, and P. K. Yegneswaran, "Adaptive Multirate Estimation and Control of Nutrient Levels in a Fed-batch Fermentation Using Off-Line and On-Line Measurements," *Can. J. Chem. Eng.*, **75**, 562 (1997).

James, S. C., R. L. Legge, and H. Budman, "On-Line Estimation in Bioreactors: A Review," *Can. Rev. Chem. Eng.*, **16**, 311 (2000).

Lombardi, M., K. Fiaty, and P. Laurent, "Implementation of Observer for On-Line Estimation of Concentration in Continuous-Stirred Membrane Bioreactor: Application to the Fermentation of Lactose," *Chem. Eng. Sci.*, **54**, 2689 (1999).

Mutha, R. K., W. R. Cluett, and A. Penlidis, "A New Multirate-Measurement-Based Estimator: Emulsion Copolymerization Batch Reactor Case Study," *Ind. Eng. Chem. Res.*, **36**, 1036 (1997a).

Mutha, R. K., W. R. Cluett, and A. Penlidis, "On-Line Nonlinear Model-Based Estimation and Control of a Polymer Reactor," *AIChE J.*, **43**, 3042 (1997b).

Ogunnaike, B. A., "Problems and Challenges of Industrial Process Control: A Commercial Polymerization Reactor Case Study," *Proc. IEEE/IFAC Joint Symp. on Computer-Aided Control System Design*, IEEE, Tucson, AZ, p. 27 (1994a).

Ogunnaike, B. A., "On-Line Modeling and Predictive Control of an Industrial Terpolymerization Reactor," *Int. J. Control*, **59**, 711 (1994b).

Radhakrishnan, T. K., K. Gangiah, and K. Y. Rani, "Multirate Multivariable Self-Tuning Control of Distillation Columns Using Kalman Predictor," *Chem. Eng. Commun.*, **127**, 55 (1994).

Robertson, D. G., J. H. Lee, and J. B. Rawlings, "A Moving Horizon-Based Approach for Least Squares State Estimation," *AIChE J.*, **42**, 2209 (1996).

Russo, L. P., and R. E. Young, "Moving-Horizon State Estimation Applied to an Industrial Polymerization Process," *Proc. American Control Conference*, San Diego, p. 1129 (1999).

Schmidt, A. D., and W. H. Ray, "The Dynamic Behavior of Continuous Polymerization Reactors—I Isothermal Solution Polymerization in a CSTR," *Chem. Eng. Sci.*, **36**, 1401 (1981).

Stone, K. M., N. F. Thornhill, F. W. Roche, and N. M. Fish, "A Method of Using Off-Line Measurements in an On-Line Estimator of Biomass Concentration for a Penicillin Fermentation and Its Effects on the Quality of the Estimates," *Proc. IFAC Symp. on Modeling and Control of Biotechnological Processes* and *Int. Conf. on Control Applications to Fermentation Technology*, Keystone, CO (1992).

Tatiraju, S., M. Soroush, and B. A. Ogunnaike, "Multi-Rate Nonlinear State Estimation with Application to a Polymerization Reactor," *AIChE J.*, **45**, 769 (1999a).

Tatiraju, S., M. Soroush, and R. Mutharasan, "Multi-Rate State and Parameter Estimation in a Biochemical Reactor," *Biotechnol. Bioeng.*, **63**, 22 (1999b).

Tatiraju, S., and M. Soroush, "Nonlinear State-Estimation in a Polymerization Reactor," *Ind. Eng. Chem. Res.*, **36**, 2679 (1997).

Urretabizkaia, A., J. R. Leiza, and J. M. Asua, "On-Line Terpolymer Composition Control in Semicontinuous Emulsion Polymerization," *AIChE J.*, **40**, 1850 (1994).

VAZO Product Bulletin, E. I. DuPont de Nemours, Philadelphia (1989).

Von Schalien, R., K. Fagervik, B. Saxen, K. Ringbom, and M. Rydstrom, "Adaptive On-Line Model for Aerobic *Saccharomyces cerevisiae* Fermentation," *Biotechnol. Bioeng.*, **48**, 631 (1995).

Zambare, N., M. Soroush, and B. A. Ogunnaike, "A Method of Robust Multi-Rate State Estimation," *J. Process Control*, in press (2002).

Manuscript received May 23, 2001, and revision received Oct. 12, 2001.